Phase relations in the Longyearbyen CO_2 Lab reservoir – forecasts for CO_2 injection and migration

Rohaldin Miri, Helge Hellevang, Alvar Braathen & Per Aagaard

Miri, R., Hellevang, H., Braathen, A. & Aagaard, P.: Phase relations in the Longyearbyen CO_2 Lab reservoir – forecasts for CO_2 injection and migration. *Norwegian Journal of Geology,* Vol 94, pp. 217–232. Oslo 2014. ISSN 029-196X.

Understanding of fluid-mixture properties relevant to the Longyearbyen CO_2 Lab pilot project (LYBCO2) is of great importance for the assessment of the injection performance. Phase equilibria and density of the binary, ternary and quaternary systems containing CO_2, CH_4, H_2O and NaCl were investigated using a Statistical Associating Fluid Theory (SAFT)-based equation of state (EoS) at ambient temperature and pressure, and salt concentrations up to 5 mol kgw^{-1}, all relevant to LYBCO2. Binary interaction parameters of the subsystems (CO_2–CH_4, CH_4–H_2O, and CH_4–NaCl) were tuned against available experimental data, using previously adjusted parameters for pure components and CO_2–H_2O subsystems. Solubility of CH_4 and CO_2 and subsequent mixture densities were predicted at 298 K and pressure up to 100 bar. It is found that by increasing the hydrocarbon in the injection stream (even in small amounts) and also the salt concentration and solubility of the CO_2 in the aqueous phase, then consequently the density of the mixture will reduce. Moreover, hydrocarbon impurities like CH_4 would result in a favourable density difference and faster plume migration; however, the probability of a three-phase state (two liquid and one vapour phase) near the bubble line is very high too. The results of this work are applicable to estimation of storage capacity as well as simulation of plume migration and fate in all projects involving a CO_2, CH_4, H_2O and NaCl-bearing fluid system.

Rohaldin Miri, Helge Hellevang, Alvar Braathen, Per Aagaard, Department of Geosciences, University of Oslo, Pb. 1047, Blindern, 0316 Oslo, Norway.

E-mail corresponding author (Helge Hellevang): helge.hellevang@geo.uio.no

Published December 24. 2014.

Introduction

Longyearbyen in Svalbard, Arctic Norway, is situated in the high arctic at 78° North. This small, isolated town has ambitions to become a carbon-neutral community by 2025 (Sand & Braathen, 2006). This will be accomplished by modifying or building a new coal-fired power plant with carbon capture technology, thereby handling the foremost local source of CO_2 emission (*c.* 65 ktons $year^{-1}$). Captured CO_2 will be stored underground by injection in nearby wells. In order to realise this ambition, the Longyearbyen CO_2 Lab pilot project (LYBCO2) has drilled and cored eight wells (Dh1 to Dh8) which, together with seismics and other studies, have been used to characterise the subsurface conditions.

The targeted reservoir is tight, with a dual porosity made up of secondary pore space and natural fractures (Fig. 1). Water injection tests suggest flow mainly in fractures. Well tests have also documented a subhydrostatic reservoir pressure, and flow of natural gas into wells.

This contribution addresses the behaviour of injected CO_2 in the reservoir, thereby giving a significant contribution to the forecast of CO_2 plume behaviour and ultimate fate. At the time of CO_2 injection, mixing with the hydrocarbons will change fluid-phase properties such as density, viscosity and critical point, and may even lead to three-phase equilibria (one gas and two liquids). In order to prepare for the future CO_2 storage in Longyearbyen, we therefore need to establish a comprehensive understanding of the properties of possible fluid mixtures relevant for the targeted storage sandstones. In this case we analyse the LYBCO2 reservoir, but our modelling results are equally relevant for other similar sites.

Geological setting

Svalbard offers a comprehensive record of bedrock, spanning from pre-Caledonian and Caledonian basement to Tertiary foreland deposits (e.g., Steel & Worsley, 1984). Of relevance for this study and the Longyearbyen CO_2 Lab are the properties of the Mesozoic stratigraphic succession, consisting of a layered sequence of mainly marine sandstones and shales. This succession was buried to 2–4 km depth (Senger et al., 2014) during development of the

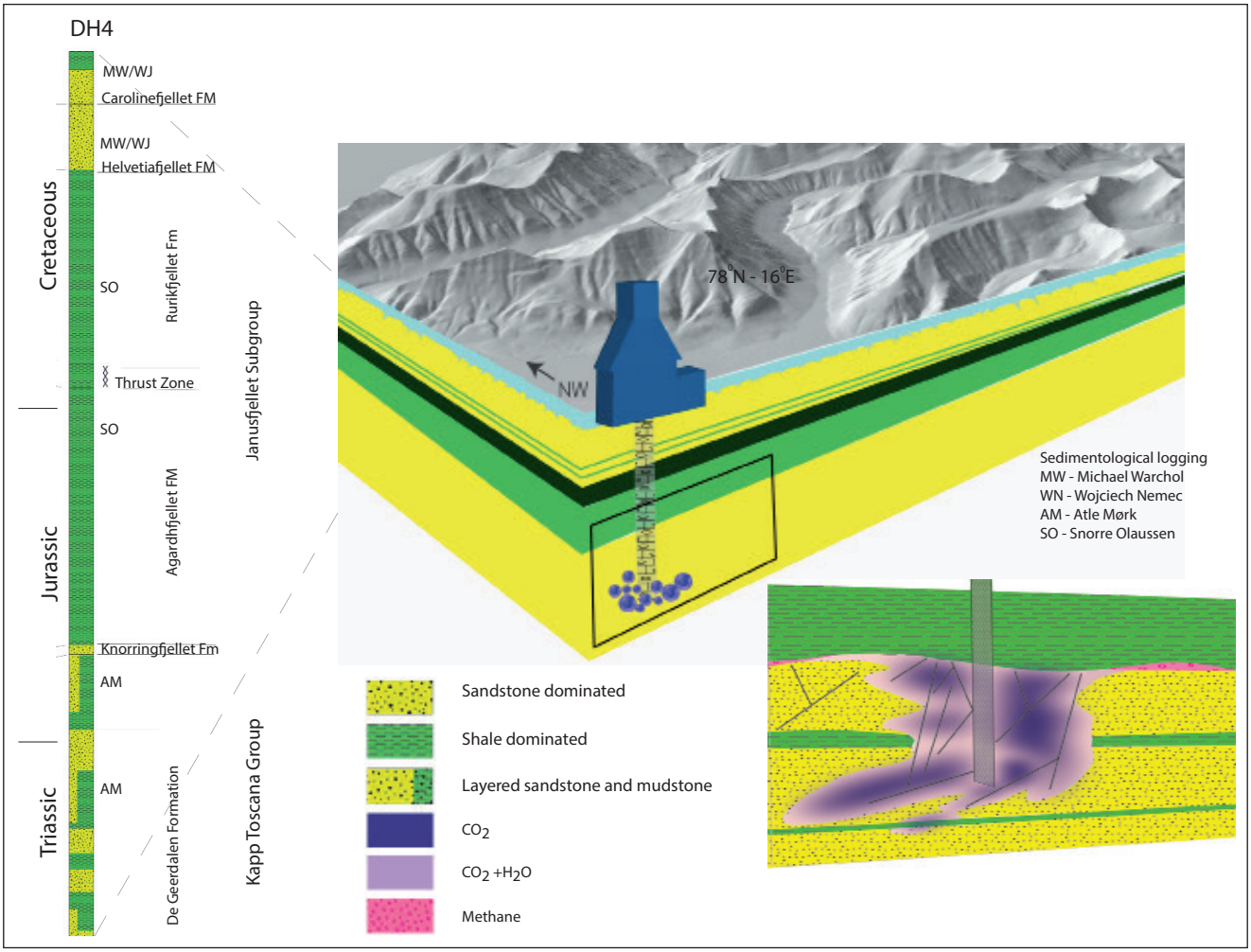

Figure 1. *Sketch of the Longyearbyen CO_2 Lab (Svalbard), illustrating the framework for CO_2 injection into reservoir sandstones at 670–970 m depth. The forecasted CO_2 plume will interact with groundwater and possibly methane gas. The explored stratigraphic succession is shown in the column to the right, with the top-seal given by the Janusfjellet Subgroup and the reservoir by the Kapp Toscana Group. The upper 120–150 m of the near-surface overburden is in the permafrost, shown with blue colour in the sketch.*

West Spitsbergen fold-and-thrust belt, as the region experienced crustal thickening, mostly in the west, and became overlain by a Palaeogene foredeep to wedge-top basin farther east (Helland-Hansen, 2010; Braathen et al., 2012). Deep burial has caused extensive diagenesis, and porous rocks mostly show secondary porosity from mineral dissolution (Mørk, 2013). Another impact of the folding and thrusting was the formation of tectonic fractures, which are widespread in mechanically stiffer units (Braathen et al., 2012; Ogata et al., 2012).

Exploration of the reservoir and cap rocks by the LYBCO2 has mostly taken place in Adventdalen *c.* 6 km from Longyearbyen and at the power station, where six out of eight wells have been drilled. The targeted succession is the Upper Triassic to Middle Jurassic De Geerdalen and Knorringfjellet formations, found at 670 to *c.* 1000 m depth in this area (Braathen et al., 2012; Ogata et al., 2012), as shown in Fig. 1. The deeper unit, the De Geerdalen Formation, consists of mainly shallow-marine to paralic sandstones interlayered with mudstones and shales (e.g., Mørk et al., 1982; Mørk & Worsley, 2006), offering a net to gross of 25–30%. The overlying Knorringfjellet Formation represents a condensed succession of shallow-marine to coastal sandstones, mudstones and some shales, with a thickness of *c.* 23 m. Net to gross is better than farther down, reaching 50%. These two units make up the so-called reservoir, which is a layered succession with probable, internal, layer-parallel seals. Sandstones offer porosities between 8 and 20% and a low matrix permeability (<2 mD), of which the Knorringfjellet Formation seems to have the most promising properties (Braathen et al., 2012; Farokhpoor et al., 2013; Mørk, 2013; Magnabosco et al., 2014).

Above the reservoir, more than 400 m of marine black shales and mudstones of the Jurassic Agardhfjellet and Rurikfjellet formations (e.g., Dypvik et al., 1991; Midtkandal & Nystuen, 2009) make up the primary top seal. Some of these shales have a high organic content, representing a regional source rock and a potential source to gas encountered in LYBCO2 wells. The overlying Helvetiafjellet Formation is made up of fluvial sandstones

grading upward into shallow-marine to offshore sandstones and shales of the Carolinefjellet Formation (Nemec et al., 1988; Gjelberg & Steel, 1995; Midtkandal & Nystuen, 2009). The Helvetiafjellet Formation shows good permeability (in fractures) and is slightly over-pressured in the drilled wells of Adventdalen. It makes up a shallow aquifer that can be used as a monitoring level during CO_2 injection (Braathen et al., 2012). All units above this level are encased in the permafrost, in which most fluids are frozen, reaching a depth of 120–150 m as recorded in the wells.

Water injection tests have been used to verify injectivity and storability of the reservoir. However, as the operational setup for tests has not allowed for production, the in situ reservoir fluid is anticipated to be brine, but no water has been produced and tested. On the other hand, the water injection tests suggest that some units have moderate to good injectivity, in contrast to analyses of drilled plugs and by Miniperm recordings of sandstone properties (Magnabosco et al., 2014). Furthermore, well-test-derived pressure data show anomalously low values even with corrections for the present-day permafrost depth (Braathen et al., 2012; Larsen, 2013a). This can only be explained if the reservoir is compartmentalised and lacks hydraulic communication with the surface. Furthermore, the geothermal gradient in the area is fairly high, with average values close to 32°C km-1. There is also another factor that may play an important role in the migration of stored CO_2; light hydrocarbons are present in the reservoir and/or cap rocks, as seen by gas flow into exploration wells (Larsen, 2013b). Mixing of injected CO_2 with the hydrocarbons will change fluid phase properties and may even lead to three-phase equilibria (one gas and two liquids). As the Longyearbyen CO_2 Lab prepares for CO_2 storage, a comprehensive understanding of the physical properties expected for gas and fluid phases in the reservoir is critical in forecasting plume behaviour. Herein, we address possible fluid mixtures and their properties which are of direct relevance for the LYBCO2 reservoir.

Scientific background

In this study we apply experimental data for binary mixtures in a wide temperature and pressure range:

CO_2–H_2O (Wiebe & Gaddy, 1939; Wiebe, 1941; Nighswander et al., 1989; Kiepe et al., 2002; Chapoy et al., 2004).

CO_2–CH_4 (Donnelly & Katz, 1954; Reamer & Sage, 1963; Kaminishi et al., 1968; Arai et al., 1971; Davalos et al., 1976; Mraw et al., 1978; Turek et al., 1984; Sretenskaya et al., 1986; Thiery et al., 1994; Seitz et al., 1996; Webster & Kidnay, 2001).

CH_4–H_2O (Michels et al., 1936; Duffy et al., 1961; Yokoyama et al., 1988; Shmonov et al., 1993; Lekvam & Bishnoi, 1997; Song et al., 1997; Dhima et al., 1998; Kiepe et al., 2003; Wang et al., 2003; Chapoy et al., 2005).

For ternary mixtures of CH_4–CO_2–H_2O and quaternary mixtures like CH_4–CO_2–H_2O–NaCl, almost no reliable experimental data are available. Therefore, developing a predictive tool to estimate phase equilibria and mixture properties of such a complex system is of significant importance. To do so, we use Statistical Associating Fluid Theory (SAFT) models for mixtures involving H_2O and CO_2.

The system of interest in this study (CH_4–CO_2–H_2O–NaCl) falls in the 'Associate Electrolyte Solutions' category with strong intermolecular, columbic and polar forces (Müller & Gubbins, 2001). Non-ideality of such a mixture can be described by two approaches: (1) activity-based approaches, which treat the non-ideality as a chemical reaction and use the Henry law or an activity model to describe the dense phase; (2) approaches based on the Statistical Association Fluid Theory (SAFT). This framework has been developed by Chapman et al. (1989) based on the molecular principles and by incorporating Wertheim's thermodynamic perturbation theory of the first order (TPT1), which is accurate for pure fluids and mixtures containing associating compounds. The main contribution in this model is developing a reference term which, unlike van der Waals equations, can capture chain length (molecular shape) and molecular association. Thanks to the inherent flexibility of this framework on assigning different reference fluids like Lennard–Jones (LJ), square-well (SW) etc., several EoS with different applications have been developed. In this study, our intention has been to apply ionic SAFT1 – which is a hetero-segmented version of SAFT developed by Adidharma & Radosz (1998) to the quaternary mixture of CH_4–CO_2–H_2O–NaCl. This model has previously been applied successfully to hydrocarbon mixtures and associating fluids. Moreover, SAFT1–RPM (Tan et al., 2005), which is an ionic version of SAFT1, was used to describe the phase equilibria and properties for CO_2–H_2O and CO_2–H_2O–NaCl systems (Ji et al., 2005). Later, SAFT1–RPM was improved to SAFT2 (Tan et al., 2006) to account for multivalent salts. Since we aim to investigate the effect of a single salt (NaCl) on phase equilibria of the CH_4–CO_2–H_2O mixture, SAFT1–RPM is best suited for this work.

The primary aim of this study was to evaluate how CO_2 interacting with saline water and light hydrocarbons (here represented by CH_4) may affect the fluid mobility in the LYBCO2 pilot. To do so, we first compared modelling results of binary and ternary mixtures to the available experimental data, and afterwards we modelled densities and phase envelopes of fluid mixtures at conditions relevant for the LYBCO2. Finally, the modelled data were discussed in relation to fluxes computed using the Darcy equation fixing all variables except the fluid densities.

Methodology

Size, shape and type of forces between the molecules of a mixture define the state and thermo-physical properties of that mixture. Standard engineering EoSs of the Van der Waals type (Peng-Robinson or Soave-Redlich-Kwong) are common choices for phase equilibria calculations of simple fluids like hydrocarbons. The most important forces in such fluids are van der Waals attractions along with weak electrostatic forces due to dipoles, quadropoles, etc. For complex fluids with strong molecular interactions, the simple repulsive reference term in engineering EoSs is not sufficient, and the predictability of phase equilibria (especially the liquid phase) is poor. SAFT type EoSs are built on a reference term which unlike Van der Waals equations can capture chain length (molecular shape) and molecular association. All SAFT versions are composed of a segment term which account for non-ideality of monomers, a chain term which captures the covalent bonding and an associating term which accounts for hydrogen bonding. Since all other thermodynamic properties can be estimated through Helmholtz free energy, it is common to formulate the SAFT EoS in terms of dimensionless residual Helmholtz energy:

$$\tilde{a}^{res} = \tilde{a}^{hs} + \tilde{a}^{dis} + \tilde{a}^{chain} + \tilde{a}^{assoc} + \tilde{a}^{ion} \quad , \qquad (1)$$

where the superscripts refer to terms accounting for the residual, hard-sphere energy per segment (calculated from the Carnahan–Starling [CS] equation), dispersion, chain, association, and ionic interactions, respectively. Since there are some errors in the original papers, a full description of the terms in the Eq. 1 is provided in the Electronic Supplement. All nomenclature is summarised in the Appendix.

Chain and association terms are basically estimated based on pair correlation functions of a reference fluid. Therefore, the heart of a SAFT EoS is the reference fluid. In SAFT1 and all subsequent versions like SAFT–RPM and square-well (SW) fluid is used as a reference. The SW fluid is defined by a steep repulsion at short distances and a short-range attraction at intermediate distances through three parameters: 1) radial distance between two segments (r); 2) the well depth (u); and 3) the reduced range of the potential well (k). The pair potential $\phi(r)$ for a SW fluid is estimated by:

$$\phi(r) = \begin{cases} \infty & r < \sigma \\ -u & \sigma \le r \le \lambda\sigma \\ 0 & r > \sigma \end{cases} \quad , \qquad (2)$$

Modelling and calibration

Adjustment of parameters

For uncharged components there are totally six adjusting parameters in the SAFT1–RPM EoS: (1) segment number m; (2) segment volume v_{oo}; (3) segment energy $u\,k^{-1}$, (4) the reduced range of the potential well λ; (5) the well depth of the association site–site potential ε; and (6) available volume for bonding κ. For charged molecules, the effective diameter d should also be adjusted to the experimental data.

In order to evaluate the phase equilibria of the quaternary mixture CH_4–CO_2–H_2O–NaCl, it is necessary to determine the adjusting parameter of SAFT1–RPM EoS for pure components together with the cross parameters and binary interaction for binary subsystems. Properties of pure molecules CH_4 (Adidharma & Radosz, 1998), CO_2 (Ji et al., 2005), H_2O (Tan et al., 2005), binary mixtures NaCl–H_2O, CO_2–H_2O and the ternary mixture CO_2–H_2O–NaCl were investigated with SAFT1 and SAFT1–RPM (Ji et al., 2005). We refer the reader to the original paper for complete results of these subsystems. In the following sections the other subsystem has been studied by the model and adjusting parameters have been derived. The average relative deviations (ARDs) used in the following sections are defined as:

$$ARD = \frac{1}{NP}\sum_{N=1}^{NP}\left(\left|1 - \frac{P_N^{cal}}{P_N^{exp}}\right|\right) \times 100 \qquad (8)$$

In this equation P could be pressure, density or mole fraction depending on the type of calculation desired. For the fitting purposes, regarding pure components, a trust region Levenberg-Marquardt algorithm is incorporated; however, for the properties of binary mixtures it has been found that the 'sum of least square' method gives enough accuracy. A list of the pure components and adjusting parameters which are used in this study is provided in Tables 1 & 2.

CH_4 (1)–CO_2 (2)

For the CH_4–CO_2 subsystem, it is assumed that carbon dioxide has three association sites, i.e., two sites of type O and one site of type C. Moreover, sites of the same type do not associate with each other. Methane is modelled as a non-associating, single segment molecule. For this system, estimation of fractions of non-bonded molecules is not analytically possible; therefore, we have implemented a generalised procedure proposed by Tan et al. (2004) to evaluate the association term. We have further assumed that the polar interaction can be represented by the association (hydrogen-bonding-type) interaction.

For the CH_4–CO_2 system, vapour liquid equilibria have been measured by Kaminishi et al. (1968) at 233.15, 253.15, 276.15 and 283.15 K and pressure from 3.7

Table 1. *Parameters for H_2O, CO_2, and CH_4.*

	m	v00(cc/mol)	u/k (K)	λ	ε/k (K)	κ
H_2O (Tan et al., 2005)	1.0000	9.48370	313.8758	1.5423	1527.72	0.058480
CO_2 (Ji et al., 2005)	1.2126	11.5845	230.4929	1.5390	581.432	0.006336
CH_4 (Adidharma & Radosz, 1998)	1.0000	15.0390	105.4800	1.7827	-	-

Table 2. *Parameters for Na^+ and Cl^- at 298.15 K (25°C).*

Ion (Tan et al., 2005)	m	v_{25}(cc/mol)	u_{25}/k (K)	λ	d_{25} (A)
Na^+	1	1.2797	3349.798	1.7	4.9373
Cl^-	1	0.7797	413.9908	1.8	

Table 3. *Data sources for CH_4–CO_2 phase equilibria and density.*

Temperature range (K)	Pressure range (MPa)	Reference	Type of data
233–283	5.27–8.18	Kaminishi et al. (1968)	x.y
224–271	1.48–7.90	Donnelly & Katz (1954)	x.y
230–270	1.52–8.52	Davalos et al. (1976)	x.y
193–219	1.38–5.69	Mraw et al. (1978)	x.y
230–270	0.89–7.112	Webster & Kidnay (2001)	x.y
310–510	0–68	Reamer & Sage (1963)	z
230	8.92–71.75	Seitz et al. (1996)	density
250	17.62–80.7		density
270	31.53–84.81		density
273.15	3.8–8.17	Arai et al. (1971)	density
288	5.2–8.01		density

up to 8.18 MPa. Similar experiments have also been performed by Davalos et al. (1976), but with a wider range of pressures from 0 up to 7.17 MPa. Webster & Kidnay (2001) have reported the phase equilibria at 230 and 270 K and pressure up to 7.14 MPa. The predicted mole fraction of methane in the gas phase in these experiments is higher than in the previous experiments at the same pressure. For this system, it is found that no binary interaction coefficient is needed for the range of temperature and pressure required for this study. The available experimental data for the CH_4–CO_2 system are listed in Table 3. The results are presented in Figs. 2, 3 & 4. Using the same set of adjusting parameters, the equilibrium compositions and compressibility factor at other temperatures are predicted without further readjustment, as shown in Figs. 5 & 6. We could predict the phase equilibrium data of Davalos et al. (1976) at 230 K and up to 70 bars with a fair accuracy (Fig. 5). We further predicted the phase equilibria at 270 K (experimental data by Davalos et al., 1976) and 288 K (experimental data by Arai et al., 1971). With increasing temperature, the accuracy of the prediction near the critical region is reduced. Fig. 6 shows agreement between the calculated and experimental compressibility factor at 510.93 K for the CO_2–CH_4 system (Reamer & Sage, 1963). Agreement is fairly good, and improves at higher CH_4 mole fractions. Between 0 and 20 MPa, errors are less than 2% at any CH_4 mole fraction. Between 20 and 40 MPa, fit errors are up to 9% at CO_2 mole fractions of above 0.7 (Fig. 6). The density of the mixture at 0.5 CH_4 mole fractions at three different temperatures were compared (Fig. 7). With increasing temperature, the density of the CH_4–CO_2 mixture decreases while pressure shows a positive effect on density. In another attempt, the coexisting density of vapour and liquid were predicted at 273 K and pressure up to 145 bar (Fig. 8); the experimental data are provided by Arai et al. (1971). The EoSs overestimate the liquid density but the gas density predictions are in fair agreement with experimental data. In the same figure, the density of a supercritical mixture is also predicted for CH_4 compositions of 0.043 and 0.116. For the 0.043 methane mole fraction, the predictions are considerably better than 0.116. As was explained earlier, the model predictions near the critical region are not fair enough.

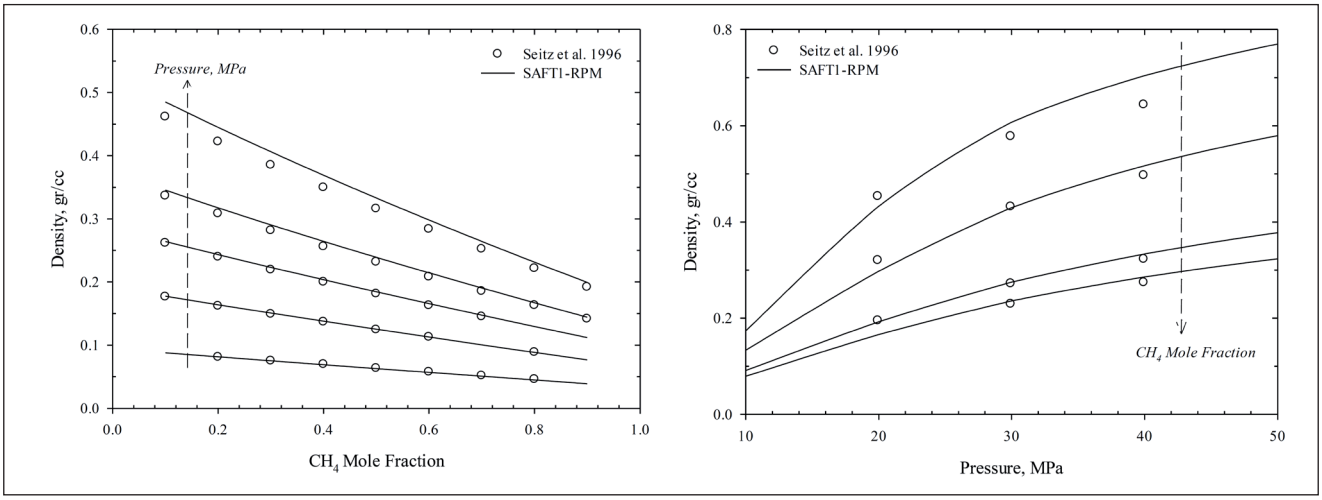

Figure 2. *Fitting the SAFT1–RPM to the density data of CO_2–CH_4 binary mixture at constant temperature or constant composition. Left: density of the CO_2–CH_4 mixture at constant temperature of 573.15 K and 9.94, 29.94, 39.94, 59.93 and 99.93 MPa. Right: density of the CO_2–CH_4 mixture at 573.15 K and 0.9, 0.8, 0.5 and 0.3 CH_4 mole fraction. Experimental data from Seitz et al. (1996).*

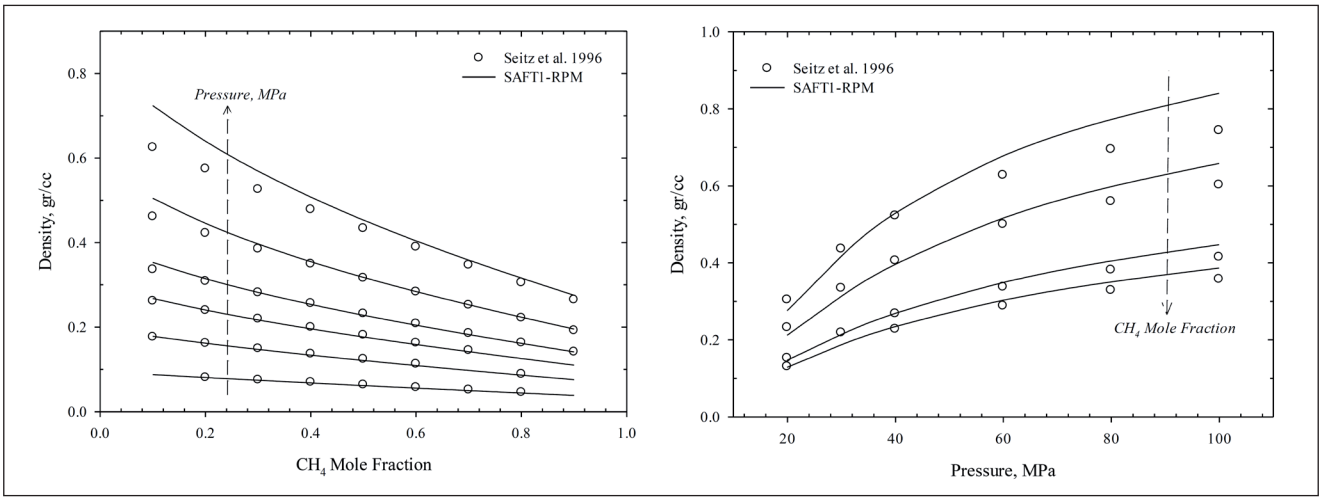

Figure 3. *Fitting the SAFT1–RPM to the density data of CO_2–CH_4 binary mixture at constant temperature or constant composition. Left: density of the CO_2–CH_4 mixture at 473.15 K and 9.94, 29.94, 39.94, 59.93, and 99.93 MPa. Right: density of the CO_2–CH_4 mixtures at 473.15 K and 0.9, 0.8, 0.5, and 0.3 CH_4 mole fraction. Experimental data: Seitz et al. (1996).*

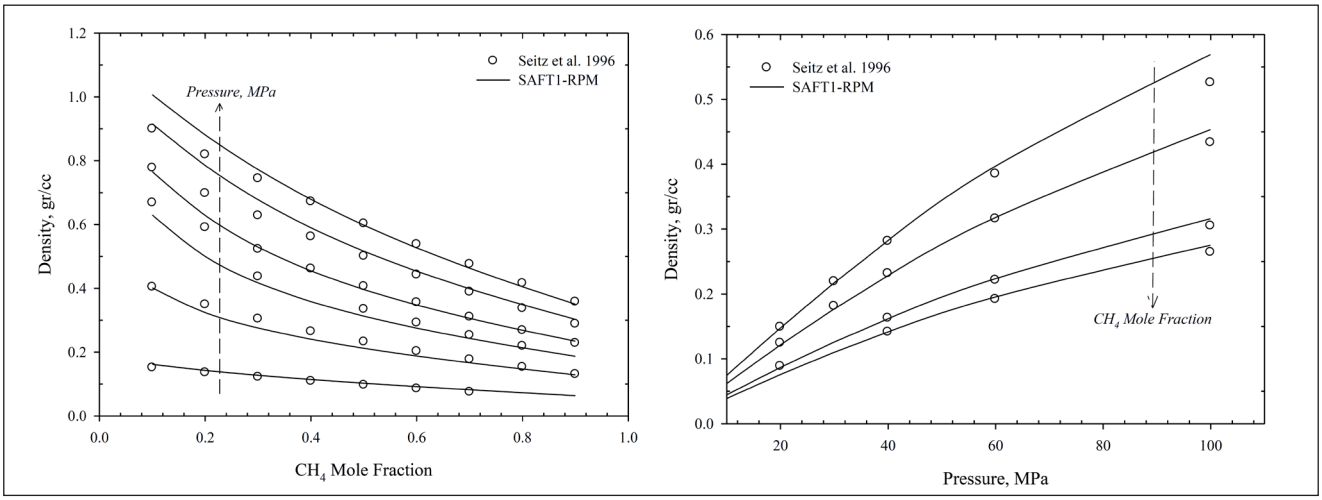

Figure 4. *Fitting the SAFT1–RPM to the density data of CO_2–CH_4 binary mixture at constant temperature or constant composition. Left: density of the CO_2–CH_4 mixture at 323.15 K and 9.94, 19.94, 39.94 and 99.93. Right: density of the CO_2–CH_4 mixture at 323.15 K and 0.9, 0.8, 0.5, and 0.3 CH_4 mole fraction. Experimental data: Seitz et al. (1996).*

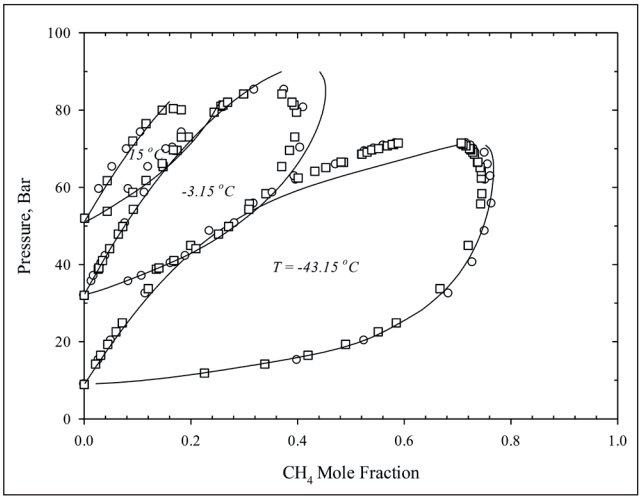

Figure 5. Vapor liquid equilibria for the CO_2–CH_4 mixture at 230, 270 K. Experimental data: 230, 270 K: Davalos et al. (1976) (circles) and Webster & Kidnay (2001) (squares), and 283.15 K: Kaminishi et al. (1968) (circles) and Donnelly & Katz (1954) (squares).

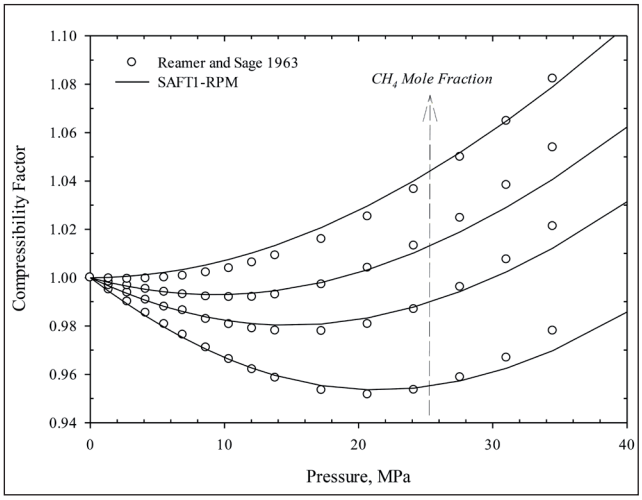

Figure 6. Compressibility factor of the CO_2–CH_4 mixture at 510.93 K and 0.6685, 0.3583, 0.1991, and 0.0852 CH_4 mole fraction. Experimental data: Reamer & Sage (1963).

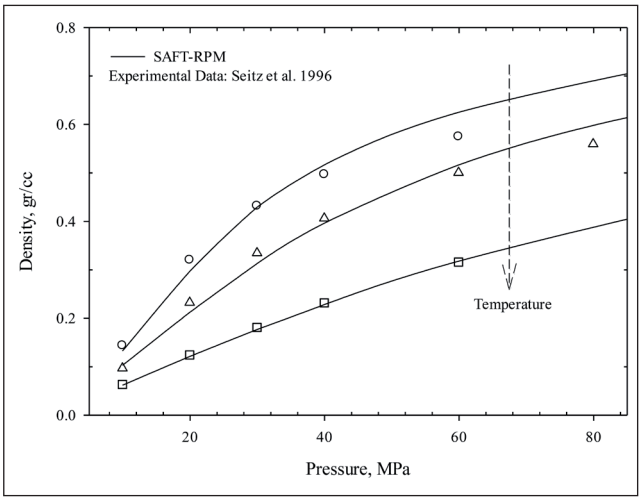

Figure 7. Density of the CO_2–CH_4 mixture at 573.15 K (circles), 473.15 K (triangles) and 323.15 K (squares) and 0.5 CH_4 mole fraction. Experimental data: Seitz et al. (1996).

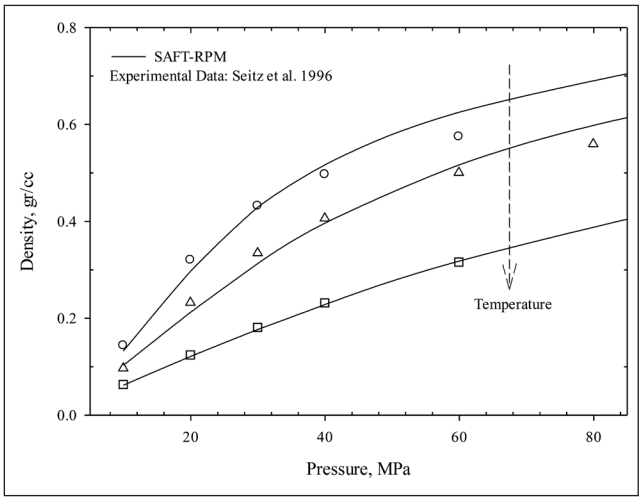

Figure 8. Coexisting densities of the CO_2–CH_4 mixture at 288.15 K. The upper line is the prediction at 0.043 CH_4 mole fraction and the lower one is at 0.116 CH_4 mole fraction. Experimental data: Arai et al. (1971) (circles).

CH_4 (1)–H_2O (3)

For this system it is assumed that H_2O has four association sites i.e., two sites of type oxygen and two sites of type hydrogen. Moreover, sites of the same type do not associate with each other. Similar to the CH_4–CO_2 mixture, methane is modelled as a non-associating, single-segment molecule. Therefore, for the CH_4–H_2O mixture only self-association of water molecules is considered. The solubility of methane in pure water has been reported extensively in the literature (Michels et al., 1936; Duffy et al., 1961; Yokoyama et al., 1988; Shmonov et al., 1993; Lekvam & Bishnoi, 1997; Song et al., 1997; Dhima et al., 1998; Kiepe et al., 2003; Wang et al., 2003; Chapoy et al., 2005). However, due to its extremely low solubility, the reported data are not entirely consistent.

The available experimental data for the CH_4–CO_2 system are listed in Table 4. In the high-pressure range, Shmonov et al. (1993) measured the phase equilibrium of the CH_4–H_2O system with temperatures up to 723 K and pressures up to 200 MPa. The experimental data reported by Sretenskaya et al. (1986) in the same region of pressure and temperature show a very good correlation with the Shmonov et al. (1993) measurements. Therefore, these two sets of data are chosen for fitting. Experimental volumetric datasets for the CH_4–H_2O fluid mixture are also listed in Table 4. A temperature-dependent binary interaction parameter k_{13} is used to adjust the cross-dispersive energy for this binary system at low temperature:

$$k_{13} = C_1 T^{-3} + C_2 T^{-2} + C_3 T^{-1} + C_4 \quad (3)$$

Table 4. *Data sources for CH_4–H_2O phase equilibria and density.*

Temperature range (K)	Pressure range (MPa)	Reference	Type
298.15	4.06–46.96	Michels et al. (1936)	x
283.2-303.2	0–40	Wang et al. (2003)	x
313.35-373.29	1.52–8.52	Kiepe et al. (2003)	x
344.15	2.5–100	Dhima et al. (1998)	x
277.8-297.6	0.491–3.865	Chapoy et al. (2005)	x,y
298.15,323.15	3.0–8.0	Yokoyama et al. (1988)	x,y
298.15-363.15	3.45	Song et al. (1997)	x,y
274.38-285.67	2.331–9.082	Lekvam & Bishnoi (1997)	x
653-723	5.0–20.0	Shmonov et al. (1993)	molar volume
653-723	5.0–20.0	Sretenskaya et al. (1986)	molar volume

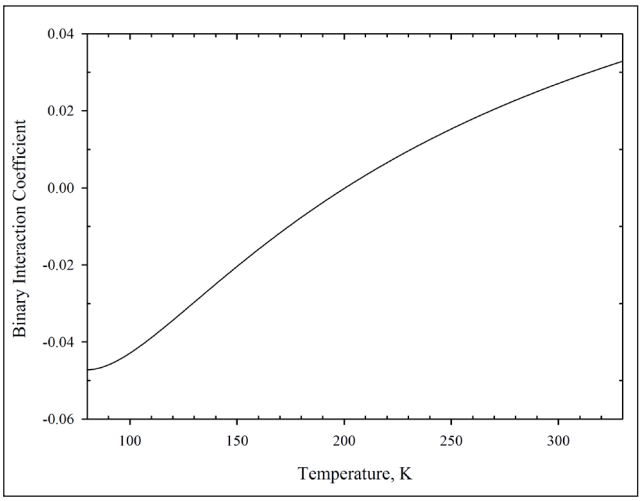

Figure 9. *Temperature-dependent binary interaction parameter k13 for H_2O–CH_4 mixture from 80 to 330 K.*

Table 5. *Fitted parameters of temperature dependent binary interaction coefficient (Eq. 2) for CH_4–CO_2 mixture*

C1	C2	C3	C4
-28624.2	1696.31	-28.9774	0.105887
Cl^-	1	0.7797	413.9908

The temperature-dependent binary interaction parameter k_{13} is fitted to molar volume for each isotherm from the several sets of experimental data reported by Sretenskaya et al. (1986) and Shmonov et al. (1993) from 653.0 K to 723.0 K (Table 4). It varies between -0.05 and 0.04 (Fig. 9). The results are presented in Table 5 and Figs. 10, 11 & 12.

Without any further adjustment, the mole fraction of CH_4 in the water-rich phase is predicted at 313.35 and 373.29 K and up to 8 MPa. The experimental data are provided by Kiepe et al. (2003). The result is presented in Fig. 13 and shows a very good agreement between the predicted and the experimental data, with an average absolute deviation error of less than 0.08 percent.

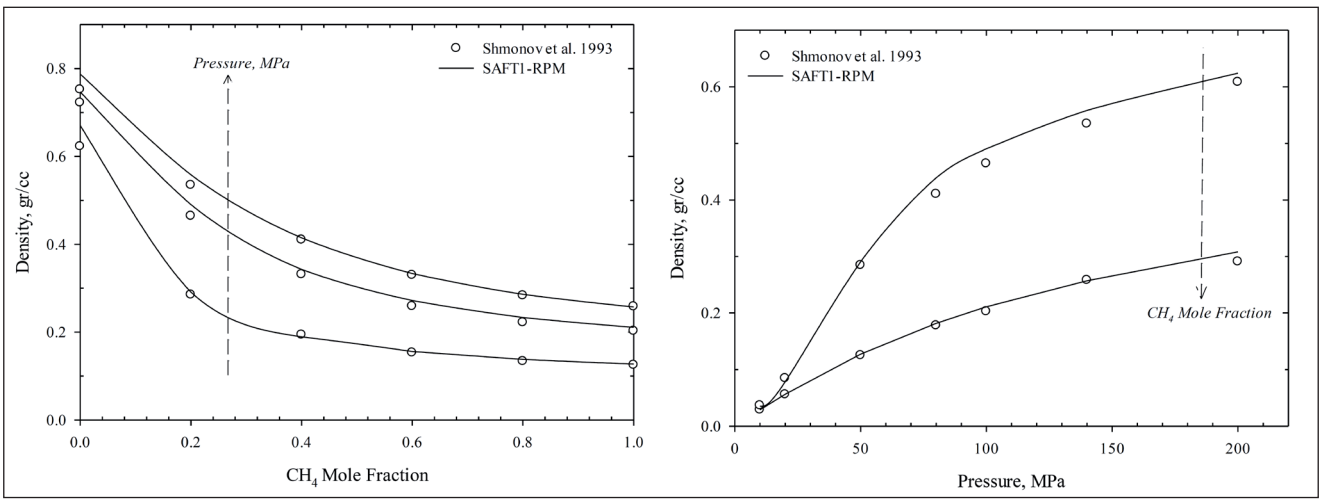

Figure 10. *Fitting the SAFT1–RPM to the density data of H_2O–CH_4 binary mixture at constant temperature or constant composition. Left: SAFT1–RPM predictions of H_2O-rich phase density for H_2O–CH_4 mixture at 653 K and 50, 100 and 200 MPa. Right: density of H2O-rich phase for H2O–CH_4 mixture at 653 K and 0.2 and 1.0 CH_4 mole fraction. Experimental data: Shmonov et al. (1993) (circles) and Sretenskaya et al. (1986) (stars).*

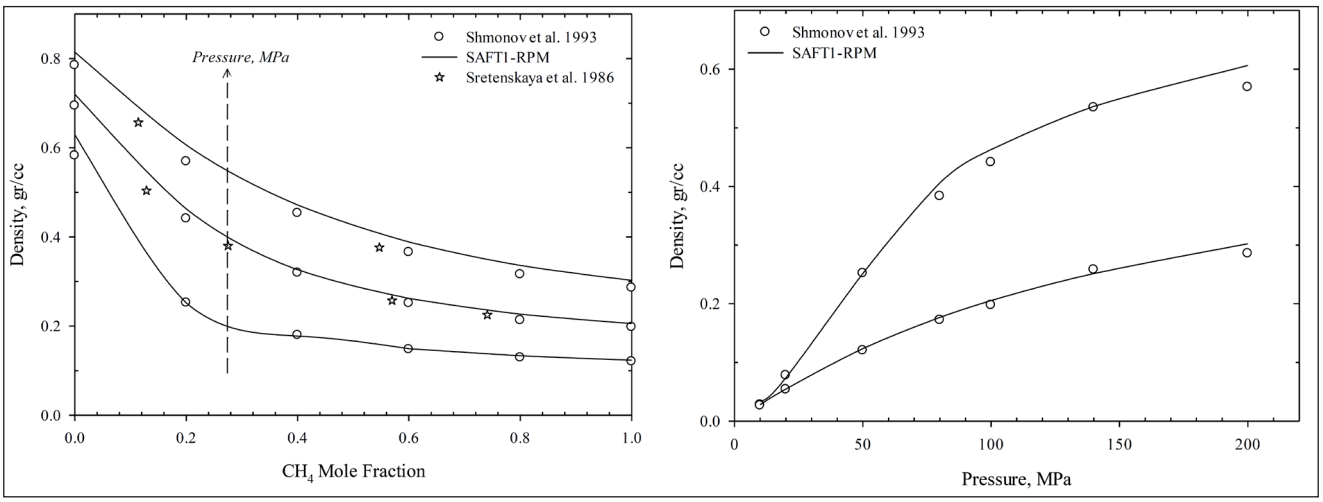

Figure 11. *Fitting the SAFT1–RPM to the density data of H_2O–CH_4 binary mixture at constant temperature or constant composition. Left: SAFT1–RPM predictions of H_2O-rich phase density for H_2O–CH_4 mixture at 673 K and 50, 80, 100 and 200 MPa. Right: density of H_2O-rich phase for H_2O–CH_4 mixture at 673 K and 0.2 and 0.1 CH_4 mole fraction. Experimental data: Shmonov et al. (1993) (circles) and Sretenskaya et al. (1986) (stars).*

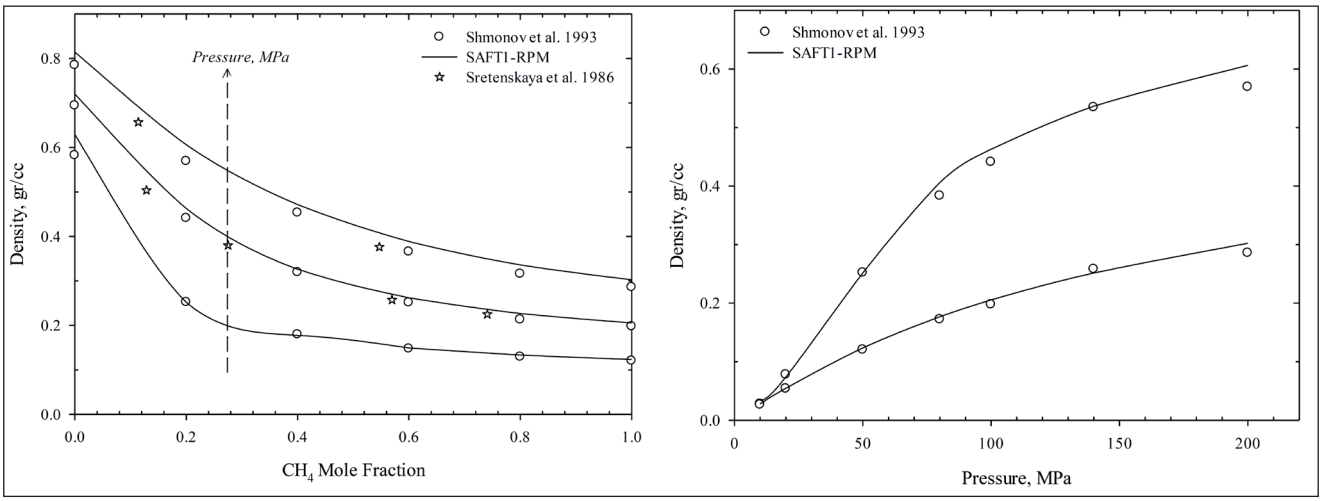

Figure 12. *Fitting the SAFT1–RPM to the density data of H_2O–CH_4 binary mixture at constant temperature or constant composition. Left: SAFT1–RPM predictions of H_2O-rich phase density for H_2O–CH_4 mixture at 723 K and 50, 80, 100 and 200 MPa. Right: density of H_2O-rich phase for H_2O–CH_4 mixture at 723 K and 0.2 and 0.1 CH_4 mole fraction. Experimental data: Shmonov et al. (1993) (circles) and Sretenskaya et al. (1986) (stars).*

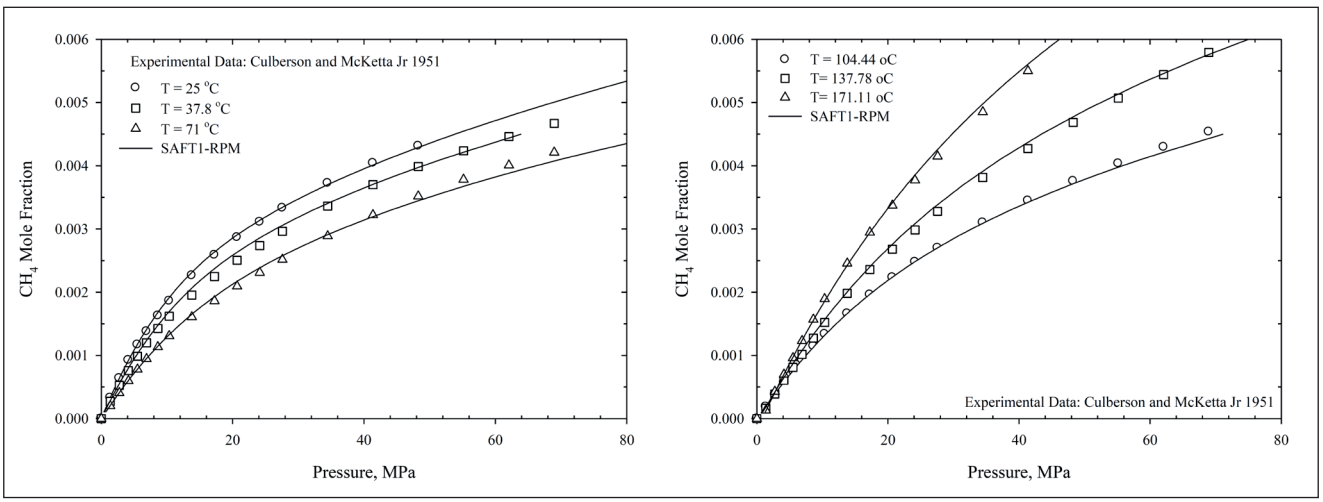

Figure 13. *SAFT1–RPM predictions of CH_4 solubility in water at different temperature and up to 80 MPa. Solid lines are SAFT1–RPM predictions and symbols are the experimental data: Culberson & McKetta Jr. (1951).*

CH_4 (1)–H_2O (3) –NaCl (4)

To account for ionic effects on the Helmholtz free energy of the mixtures containing single salts, Tan et al. (2005) suggested a coupling of the Restricted Primitive Model (RPM) (considering ions in a medium with a uniform dielectric constant) with SAFT1. He used a hybrid approach in coupling that involves both the individual-ion and the salt parameters. In this approach the aqueous electrolyte is treated as a binary solution containing water and salt, and the salt treated as a molecule composed of two different segments corresponding to the cation and the anion. The ion parameters have been adjusted to vapour pressure and density of H_2O–NaCl by Tan et al. (2005) for a wide range of pressure and temperatures. We adopted these ion parameters to further investigate the ternary mixture of CH_4–H_2O–NaCl. The ion parameters are listed in Table 2.

Phase equilibrium data for CH_4–H_2O–NaCl have been measured by several investigators (Michels et al., 1936; Yokoyama et al., 1988; Shmonov et al., 1993; Lekvam & Bishnoi, 1997; Song et al., 1997; Dhima et al., 1998; Kiepe et al., 2003; Wang et al., 2003; Chapoy et al., 2005), and some of these results are in our interest range of pressure and temperature. They are summarised in Table 4. To account for cross-dispersive energy between ions and CH_4 a binary interaction parameter is needed.

$$k_{14+,-} = 0.03376 \quad (4)$$

The solubility of CH_4 in water and aqueous solutions has been measured at pressures up to 200 atm and a salt molality up to 6 mol kg-1. Fig. 14 shows the comparison of the calculated results with the experimental data at different salt concentrations. The experimental data of Michels et al. (1936) and Duffy et al. (1961) are included in the figure. At 298 K it is confirmed that the calculated results agree with the experimental data up to 5.4 mol kg^{-1}.

Discussion

In our analysis of phase relations for the LYBCO2 pilot, several uncertainties require caution. As explained earlier, the predictive capabilities of SAFT1–RPM and the general lack of experimental data are our main motivation for using the EoS to predict the phase behaviour of the quaternary system of CH_4–CO_2–H_2O–NaCl.

Prediction of density and phase equilibria of a binary mixture of CO_2–CH_4 is of significant importance for designing carbon capture processes. This importance can be seen in almost all CCS stages from capture and combustion to transport and injection. From the storage point of view, the density of supercritical gas is also a measure of the amount of gas that can be stored at reservoir conditions (Bachu et al., 2007; Bachu, 2008; Ji & Zhu, 2012). In addition, to minimise the cost of CO_2 transport by pipelines, it is necessary to keep the pressure sufficiently high (i.e., higher density), retain a low viscosity (i.e., lower pressure drop) and to perform the whole operation in single phase (i.e., supercritical or dense liquid).

In Fig. 15, the predicted two-phase envelope of this binary system at 298 K is shown, along with 288 K. The phase split region is smaller at 298 K and the critical pressure slightly greater than for 288 K. Noticeably, in these calculations the SAFT–RPM will not successfully

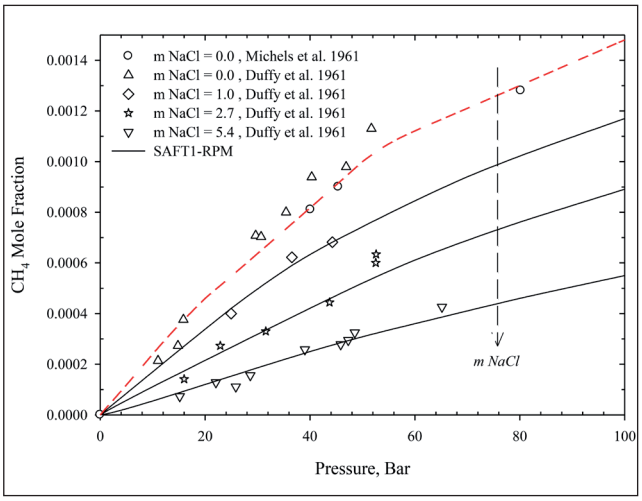

Figure 14. *Mole fraction of methane in the H_2O-rich phase for H_2O–CH_4–NaCl mixture at 298 K and NaCl molality of 0, 1, 2.7 and 5.4. Experimental data: Duffy et al. (1961) (stars) and Michels et al. (1936) (circles).*

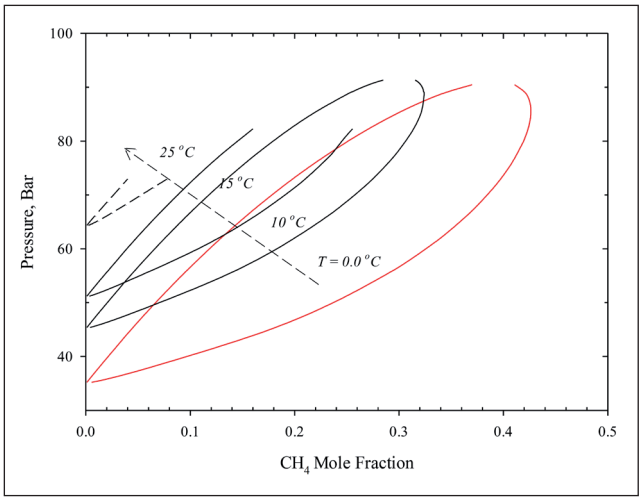

Figure 15. *SAFT1–RPM prediction of vapour liquid equilibria for CO_2–CH_4 mixture at 273.15 (0°C), 283.15 (10°C), 288.15 (15°C) and 298.15 K (25°C). The two-phase region is getting smaller as temperature increases, and accordingly the accuracy of the SAFT1–RPM predictions reduces noticeably, especially close to the critical point.*

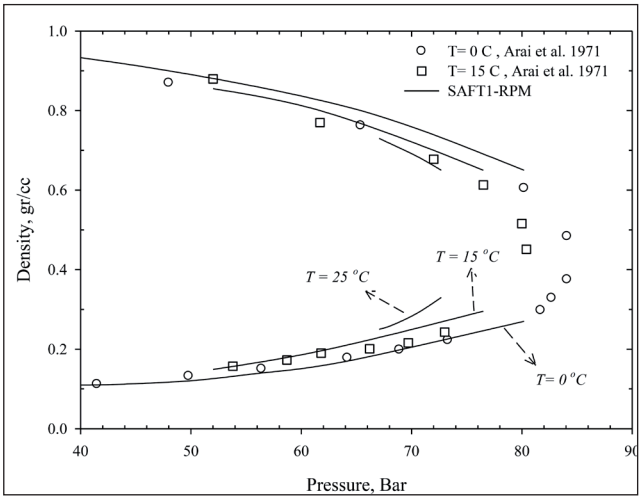

Figure 16. *SAFT1–RPM prediction of coexisting densities of CO_2–CH_4 mixture at 298 K (25°C), 288.15 K (15°C) and 273.15 K (0°C). The predictions for 288.15 K and 273.15 K are in good agreement with the experimental data of Arai et al. (1971) except in the vicinity of the critical point.*

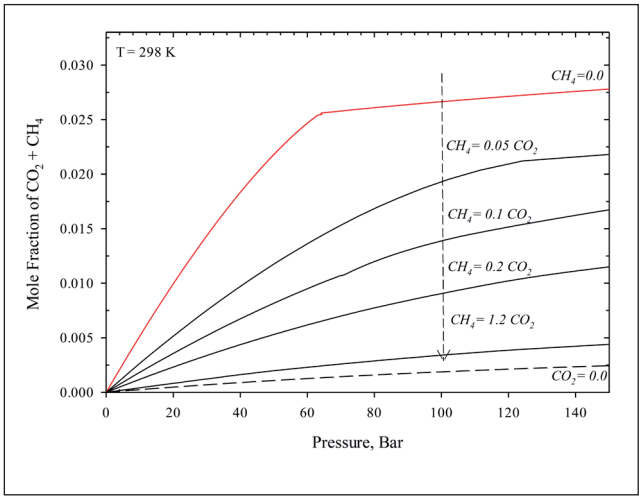

Figure 17. *The predicted equilibrium pressure by SAFT1–RPM vs. mole fraction of (CH_4 + CO_2) in the H_2O-rich phase at 298 K, zero salt content and different mole fractions of CH_4. The red and dotted lines are the solubility of the pure CO_2 and CH_4 in the water, respectively. The solubility of the gas mixture significantly decreases as the CO_2 phase is getting richer in CH_4.*

predict the phase equilibria near the critical region. At a given temperature, with an increasing methane mole fraction, the bubble and dew pressure will increase, which indicates an increase in the minimum operation conditions of a CO_2 pipeline. Moreover, at a fixed temperature, when the mole fraction of methane exceeds a critical value, a phase split will occur. As temperature increases, this critical value will decrease, which implies a narrower range of pressure and temperature to avoid two-phase flow.

An attempt was also made to predict the density of the CO_2–CH_4 subsystem. Fig. 16 shows the predicted density of the binary mixture against the experimental data of Arai et al. (1971) at 288 and 273 K. The results show a fairly good agreement with the experimental data. Therefore, we have assumed that the prediction of density at 298 K should be in the same error range for 288 and 273 K. By increasing the temperature, the density of the liquid phase is reduced and the two-phase region becomes smaller (range of 67–85 bars). In addition, an equilibrium and supercritical density of CO_2–CH_4 was illustrated at pressures of 45 to 145 bar at 298 K in Fig. 8. With inclusion of a 0.043 mole fraction of methane, a phase split will occur and density will then increase with pressure. Inclusion of more methane (≈ 0.116) still indicates a phase split; however, the predicted density is considerably decreased, i.e., the amount of gas that can be stored at reservoir conditions is smaller. Therefore, inclusion of methane even at a small fraction is not favourable with respect to storage.

Accurate determination of gas solubility in brine is essential for appropriate modelling of the physical and chemical processes occurring in porous media. CO_2 at a supercritical state shows a relatively good solubility (diffusion dominated) in water at ambient level and would increase the density of the brine. This density difference may result in density instabilities (Rayleigh-Taylor instability) and consequently plumes of CO_2-saturated water will migrate downwards, which can accelerate the mixing process as they act like eddy currents and enhance the diffusion process and solubility trapping. Dissolution of CH_4 in water has the opposite effect as it reduces the density of the aqueous solution. The solubility of CH_4 in water is very low (about 0.0015 at 298 K and 100 bar).

Using the SAFT1–RPM with the obtained adjusting parameter and without any future adjustment, the solubility of CH_4 and CO_2 in the H_2O at 298 K and pressure up to 100 bar were predicted. The results are presented in Fig. 17. It is shown that with increasing methane concentration in the injected gas, the solubility of the gas mixture decreases as methane is less soluble than CO_2. It is worth mentioning that our predictions are up to 400 bar and, if the trend is viable, a positive effect of CH_4 on the solubility might not be observed at very high pressures. To investigate further the effect of methane on the solubility of CO_2, calculations were performed with brines of different salinities. The results for salt molality of up to 5 mol kgw^{-1} (kg water) are shown in Fig. 18. Inclusion of NaCl to the water reduces the solubility of CO_2 + CH_4 considerably. Our findings suggest that for the temperature and pressure range of interest in this study, both CH_4 and NaCl have adverse effects on the solubility and consequently also on the density of the mixture.

The main important driving mechanisms in a typical carbon capture and storage process are capillary, gravity and viscous forces. In CO_2 sequestration projects

targeting sloping aquifers such as the LYBCO2, the gravity difference between the injected fluid (which is usually in a supercritical state) and the host fluid is the main driving force which controls the rate of injection and migration of the CO_2 plume. In a simple presentation of the injection process, the velocity of the front in the vertical direction (Z) can be approximated by:

$$V = \frac{-K K_{rm}}{\mu_m}\left(\frac{\partial P_C}{\partial Z} - \Delta\rho g\right) \quad (5)$$

If we further neglect the capillary pressure of the system, assuming a small entry pressure for the rock, then the maximum velocity of the front will be due to either density difference or gravity force. As discussed earlier, the addition of hydrocarbon even in small amounts would result in a considerable change in the density of the mixture resulting in a larger density contrast and consequently a faster-moving front. This effect is further illustrated in Fig. 19 for pure water at 298 K and pressure up to 100 bar. Addition of methane will reduce the density of aqueous solution dramatically and at higher pressure this effect is much more pronounced. Moreover, some experiments (Jackson, 1956; Kestin & Leidenfrost, 1959) confirmed that the viscosity of CO_2 is decreasing as the CH_4 mole fraction increases in the injection stream. Therefore, both density and viscosity have a positive effect on the mobility of the front. In addition, following the injection of gas into the reservoir there will be a pressure buildup and the average reservoir pressure will also continuously increase; therefore, it is concluded that inclusion of methane would continuously enhance the front velocity. The detailed description of the plume migration and accurate estimation of the front velocity require precise simulation of the whole process incorporating a multi-physics tool, which is out of the scope of this study. However, a less sophisticated approximation has confirmed the same conclusions about the mobility of the front as drawn here. Blanco et al. (2012) using a scaling equation combining the density difference and viscosity of the injection stream, estimated that the plume velocity can reach nearly three times that of a pure CO_2 plume as the concentration of CH_4 is increased in the CO_2 stream.

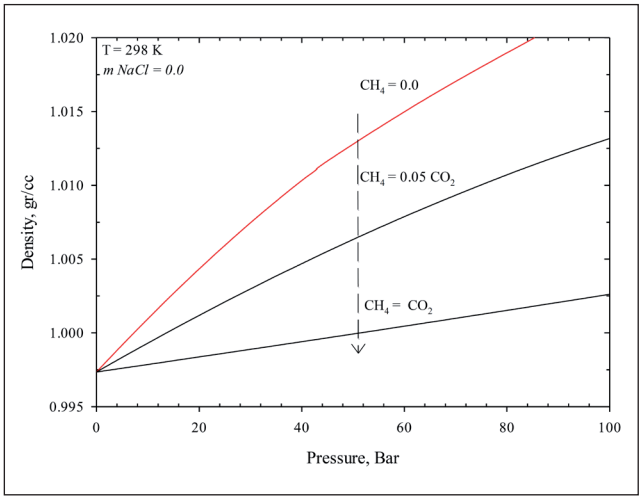

Figure 19. *Density of aqueous phase (CH_4 + CO_2 + H_2O) mixture at 298 K, zero salt content and different CH_4 concentrations. The arrow shows the direction of increasing CH_4 content in the CO_2 phase. The red line shows the aqueous phase density of the CO_2 + H_2O mixture. Even small amounts of CH_4 reduces the density considerably and the density reduction increases as pressure increases.*

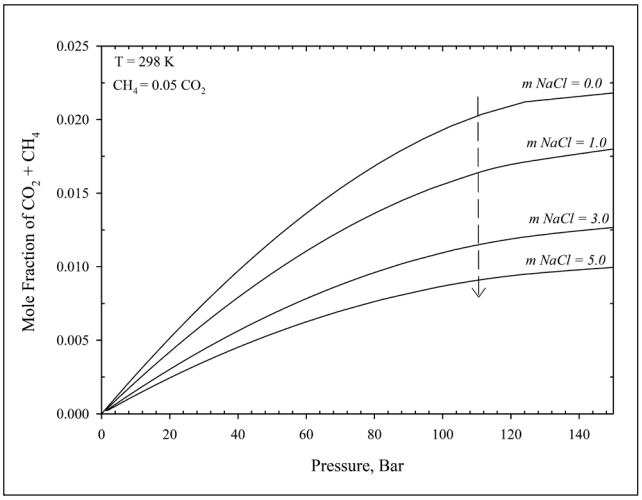

Figure 18. *The predicted equilibrium pressure by SAFT1–RPM vs. mole fraction of (CH_4 + CO_2) in the H_2O-rich phase at 298 K, constant CH_4 concentration of 0.05 × CO_2 and different salt molality. The solubility of the gas mixture reduces with increasing salt content.*

The relative permeability and capillary pressure are key elements in controlling viscous and capillary forces. In Eq. 5, relative permeability is considered to be that of the mixture, but in some cases for fluids ahead of or behind the front, three phases are in equilibrium. Developing a pressure-temperature diagram for the fluid mixture of relevance here is complicated, and is not included. However, preliminary results show a narrow three-phase region near the bubble line. Accordingly, a three-phase bubble-point procedure is required to accurately capture this region. Before CO_2 injection into the reservoir of the LYBCO2, work on the three-phase relative permeability and capillary pressure should be undertaken to further improve the simulation results that predict the plume migration.

Conclusions

Hetero-segmented SAFT EoS (SAFT1–RPM) is used to predict phase equilibria of binary and ternary mixtures containing light hydrocarbon (methane), water and carbon dioxide. Furthermore, the effect of a single salt (sodium chloride) on the behaviour of the mixture was also investigated using SAFT1–RPM. Cross-dispersive parameters between CH_4–H_2O, CH_4–ions (Na^+ and Cl^-) and CH_4–CO_2 were obtained by adjusting the phase equilibria and mixture properties of the subsystems. By using the SAFT1–RPM and obtained adjusting

parameter and without any further adjustment, the density of the mixture and solubility of CH_4 and CO_2 in the H_2O–NaCl at 298 K and pressure up to 100 bar were predicted. The results show that the solubility of the CO_2 + CH_4 in the water is less than that of CO_2 alone. Moreover, adding NaCl to the water will reduce the solubility even more. Hydrocarbon impurities like CH_4 would result in a favourable density difference and faster plume migration. However, the probability of a three-phase state (two liquid and one vapour phase) near the bubble line is very high.

Acknowledgements. Dr. Hertanto Adidharma and Dr. Sugata Tan have provided invaluable help in making and discussing the solver for the SAFT equations. Gratitude goes to the Longyearbyen CO_2 Lab with partners for stimulating and motivating this research. This work has been partly funded by the University of Oslo and the SUCCESS center for CO_2 storage under grant 193825/S60 from the Research Council of Norway (RCN). Two anonymous reviewers are thanked for comments to an earlier version of this paper.

References

Adidharma, H. & Radosz, M. 1998: Prototype of an engineering equation of state for heterosegmented polymers. *Industrial & Engineering Chemistry Research 37*, 4453–4462

Adidharma, H. & Radosz, M. 2001: SAFT1 for associating fluids: Alkanols. *The Journal of Physical Chemistry B 105*, 9822–9827

Arai, Y., Kaminishi, G. & Saito, S. 1971: The experimental determination of the PVTX relations for the Carbon dioxide-nitrogen and the carbon dioxide-methane systems. *Journal of Chemical Engineering of Japan 4*, 113–122

Bachu, S., Bonijoly, D., Bradshaw, J., Burruss, R., Holloway, S., Christensen, N.P. & Mathiassen, O.M. 2007: CO_2 storage capacity estimation: Methodology and gaps. *International Journal of Greenhouse Gas Control 1*, 430–443

Bachu, S. 2008: CO_2 storage in geological media: Role, means, status and barriers to deployment. *Progress in Energy and Combustion Science 34*, 254–273

Blanco, S.T., Rivas, C., Fernández, J., Artal, M. & Velasco, I. 2012: Influence of Methane in CO_2 Transport and Storage for CCS Technology. *Environmental Science & Technology 46*, 13016–13023

Braathen, A., Balum, K., Christiansen, H.H., Dahl, T., Eiken, O., Elvebakk, H., Hansen, F., Hanssen, T.H., Jochmann, M., Johansen, T.A., Johnsen, H., Larsen, L., Lie, T., Mertes, J., Mork, A., Mork, M.B., Nemec, W., Olaussen, S., Oye, V., Rod, K., Titlestad, G.O., Tveranger, J. & Vagle, K. 2012: The Longyearbyen CO_2 Lab of Svalbard, Norway—initial assessment of the geological conditions for CO_2 sequestration. *Norwegian Journal of Geology 92*, 353–376

Carnahan, N.F. & Starling, K.E. 1969: Equation of state for nonattracting rigid spheres. *The Journal of Chemical Physics 51*, 635–636

Chapman, W.G., Gubbins, K.E., Jackson, G. & Radosz, M. 1989: SAFT: Equation-of-state solution model for associating fluids. *Fluid Phase Equilibria 52*, 31–38

Chapoy, A., Mohammadi, A.H., Tohidi, B. & Richon, D. 2005: Estimation of water content for methane+ water and methane+ ethane+ n-butane+ water systems using a new sampling device. *Journal of Chemical & Engineering Data 50*, 1157–1161

Culberson, O. & McKetta Jr, J. 1951: Phase Equilibria in Hydrocarbon-Water Systems III-The Solubility of Methane in Water at Pressures to 10000 PSIA. *Journal of Petroleum Technology 3*, 223–226

Davalos, J., Anderson, W.R., Phelps, R.E. & Kidnay, A.J. 1976: Liquid-vapor equilibria at 250.00. deg. K for systems containing methane, ethane, and carbon dioxide. *Journal of Chemical and Engineering Data 21*, 81–84

Dhima, A., de Hemptinne, J.-C. & Moracchini, G. 1998: Solubility of light hydrocarbons and their mixtures in pure water under high pressure. *Fluid Phase Equilibria 145*, 129–150

Donnelly, H.G. & Katz, D.L. 1954: Phase equilibria in the carbon dioxide–methane system. *Industrial & Engineering Chemistry 46*, 511–517

Duffy, J.R., Smith, N.O. & Nagy, B. 1961: Solubility of natural gases in aqueous salt solutions-I: Liquidus surfaces in the system CH_4–H_2O–$NaCl_2$–$CaCl_2$ at room temperatures and at pressures below 1000 psia. *Geochimica et Cosmochimica Acta 24*, 23–31, doi: http://dx.doi.org/10.1016/0016–7037(61)90004–7.

Dypvik, H., Eikeland, T., Backer, O., K., Andresen, A., Johanen, H., Elverhøi, A., Nagy, J., Haremo, P. & Biærke, T. 1991: The Janusfjellet Subgroup (Bathonian to Hauterivian) on central Spitsbergen: a revised lithostratigraphy. *Polar Research 9*, 21–44

Farokhpoor, R., Lindeberg, E.G.B., Torsæter, O., Mørk, M.B. & Mørk, A. 2013: Permeability and relative permeability measurements for CO_2-brine system at reservoir conditions in low permeable sandstones in Svalbard. *Greenhouse Gases: Science and Technology.*

Gjelberg, J. & Steel, R.J. 1995: Helvetiafjellet Formation (Barremian–Aptian), Spitsbergen: characteristics of a transgressive succession. *Norwegian Petroleum Society Special Publications 5*, 571–593

Helland-Hansen, W. 2010: Facies and stacking patterns of shelf-deltas within the Palaeogene Battfjellet Formation, Nordenskiöld Land, Svalbard: implications for subsurface reservoir prediction. *Sedimentology 57*, 190–208

Jackson, W.M. 1956: Viscosities Of The Binary Gas Mixtures, Methane-Carbon Dioxide And Ethylent-Argon. *The Journal of Physical Chemistry 60*, 789–791

Ji, X., Tan, S.P., Adidharma, H. & Radosz, M. 2005: SAFT1–RPM approximation extended to phase equilibria and densities of CO_2–H_2O and CO_2–H_2O–NaCl systems. *Industrial & Engineering Chemistry Research 44*, 8419–8427

Ji, X. & Adidharma, H. 2012: Prediction of molar volume and partial molar volume for CO_2/ionic liquid systems with heterosegmented statistical associating fluid theory. *Fluid Phase Equilibria 315*, 53–63

Ji, X. & Zhu, C. 2012: Predicting possible effects of H2S impurity on CO_2 transportation and geological storage. *Environmental Science & Technology 47*, 55–62

Kaminishi, G.I., Arai, Y., Shozaburo, S. & Maeda, S. 1968: Vapor-liquid equilibria for binary and ternary systems containing carbon dioxide. *Journal of Chemical Engineering of Japan 1*, 109–116

Kestin, J. & Leidenfrost, W. 1959: The effect of pressure on the viscosity of N_2CO_2 mixtures. *Physica 25*, 525–536, doi: http://dx.doi.org/10.1016/S0031–8914(59)95498–9.

Kiepe, J., Horstmann, S., Fischer, K. & Gmehling, J. 2003: Experimental determination and prediction of gas solubility data for methane+ water solutions containing different monovalent electrolytes. *Industrial & Engineering Chemistry Research 42*, 5392–5398

Larsen, L. 2013a: Analyses of DH4 Upper Zone Injection and Falloff Data, September 5 – October 15, 2013, 22 pp.

Larsen, L. 2013b: Gas Test Analyses of DH5R Flow and Shut-In Data September 2012 –October 2013, 32 pp.

Lekvam, K. & Bishnoi, P.R. 1997: Dissolution of methane in water at low temperatures and intermediate pressures. *Fluid Phase Equilibria 131*, 297–309

Magnabosco, C., Braathen, A. & Ogata, K. 2014: Permeability model of tight sandstones – calibration based in integrated permeability analysis of the Longyearbyen CO_2 lab reservoir sandstones. *Norwegian Journal of Geology 94*, 189–200

Michels, A., Gerver, J. & Bijl, A. 1936: The influence of pressure on the solubility of gases. *Physica 3*, 797–808

Midtkandal, I. & Nystuen, J. 2009: Depositional architecture of a low-gradient ramp shelf in an epicontinental sea: the lower Cretaceous of Svalbard. *Basin Research 21*, 655–675

Mørk, A., Knarud, R. & Worsley, D. 1982: Depositional and diagenetic environments of the Triassic and Lower Jurassic succession of Svalbard. *Arctic Geology and Geophysics: Proceedings of the Third International Symposium on Arctic Geology — Memoir 8*, pp. 371–398.

Mørk, A. & Worsley, D. 2006: Triassic of Svalbard and the Barents shelf. *NGF Abstracts and Proceedings 3*, 23–29

Mørk, M.B.E. 2013: Diagenesis and quartz cement distribution of low-permeability Upper Triassic–Middle Jurassic reservoir sandstones, Longyearbyen CO_2 lab well site in Svalbard, Norway. *American Association of Petroleum Geologists Bulletin 97*, 577–596

Mraw, S.C., Hwang, S.C. & Kobayashi, R. 1978: Vapor-liquid equilibrium of the methane-carbon dioxide system at low temperatures. *Journal of Chemical and Engineering Data 23*, 135–139

Müller, E.A. & Gubbins, K.E. 2001: Molecular-based equations of state for associating fluids: A review of SAFT and related approaches. *Industrial & Engineering Chemistry Research 40*, 2193–2211

Nemec, W., Steel, R., Gjelberg, J., Collinson, J., Prestholm, E. & Oxnevad, I. 1988: Anatomy of collapsed and re-established delta front in Lower Cretaceous of eastern Spitsbergen: gravitational sliding and sedimentation processes. *American Association of Petroleum Geologists Bulletin 72*, 454–476

Ogata, K., Senger, K., Braathen, A., Tveranger, J. & Olaussen, S. 2012: The importance of natural fractures in a tight reservoir for potential CO_2 storage: case study of the upper Triassic to middle Jurassic Kapp Toscana Group (Spitsbergen, Arctic Norway). *In* G.H. Spence, J. Redfern, R. Aguilera, T.G. Bevan, J.W. Cosgrove, G.D. Couples & J.-M. Daniel (eds.): *Advances in the Study of Fractured Reservoirs*, Geological Society of London Special Publication 374. Geological Society of London, doi:10.1144/SP374.9.

Reamer, H. & Sage, B. 1963: Phase equilibria in hydrocarbon systems. Volumetric and phase behavior of the n-decane-CO_2 system. *Journal of Chemical and Engineering Data 8*, 508–513

Sand, G. & Braathen, A. 2006: CO_2-fritt Svalbard i 2025? . *In*: Svalbardposten, 10 November.

Seitz, J.C., Blencoe, J.G. & Bodnar, R.J. 1996: Volumetric properties for {(1−x) CO_2+ xCH_4},{(1−x) CO_2+ xN_2}, and {(1−x) CH_4+xN_2} at the pressures (9.94, 19.94, 29.94, 39.94, 59.93, 79.93, and 99.93) MPa and temperatures (323.15, 373.15, 473.15, and 573.15) K. *The Journal of Chemical Thermodynamics 28*, 521–538

Senger, K., Planke, S., Polteau, S., Ogata, K. & Svensen, H. 2014: Sill emplacement and contact metamorphism of a siliciclastic reservoir on Svalbard, Arctic Norway. *Norwegian Journal of Geology 94*, 155–169.

Shmonov, V.M., Sadus, R.J. & Franck, E.U. 1993: High-pressure phase equilibria and supercritical pVT data of the binary water+ methane mixture to 723 K and 200 MPa. *The Journal of Physical Chemistry 97*, 9054–9059

Song, K., Feneyrou, G., Fleyfel, F., Martin, R., Lievois, J. & Kobayashi, R. 1997: Solubility measurements of methane and ethane in water at and near hydrate conditions. *Fluid Phase Equilibria 128*, 249–259

Sretenskaya, N.G., Zakirov, I.V., Shmonov, V.M. & Shmulovich, K.I. 1986: *Experiment in solution of actual problems of geology*, Nauka Publishing House, pp. 315–334

Steel, R.J. & Worsley, D. 1984: Svalbard's post-Caledonian strata—an atlas of sedimentational patterns and palaeogeographic evolution: *Petroleum geology of the North European margin*, Springer, pp. 109–135.

Tan, S.P., Adidharma, H. & Radosz, M. 2004: Generalized procedure for estimating the fractions of nonbonded associating molecules and their derivatives in thermodynamic perturbation theory. *Industrial & Engineering Chemistry Research 43*, 203–208

Tan, S.P., Adidharma, H. & Radosz, M. 2005: Statistical associating fluid theory coupled with restricted primitive model to represent aqueous strong electrolytes. *Industrial & Engineering Chemistry Research 44*, 4442–4452

Tan, S.P., Ji, X., Adidharma, H. & Radosz, M. 2006: Statistical associating fluid theory coupled with restrictive primitive model extended to bivalent ions. SAFT2: 1. single salt+ water solutions. *The Journal of Physical Chemistry B 110*, 16694–16699

Thiery, R., Vidal, J. & Dubessy, J. 1994: Phase equilibria modelling applied to fluid inclusions: Liquid-vapour equilibria and calculation of the molar volume in the CO_2–CH_4–N2 system. *Geochimica et Cosmochimica Acta 58*, 1073–1082

Turek, E., Metcalfs, R., Yarborough, L. & Robinson Jr, R. 1984: Phase equilibria in CO_2-multicomponent hydrocarbon systems: experimental data and an improved prediction technique. *Old SPE Journal 24*, 308–324

Wang, L.K., Chen, G.J., Han, G.H., Guo, X.Q. & Guo, T.M. 2003: Experimental study on the solubility of natural gas components in water with or without hydrate inhibitor. *Fluid Phase Equilibria 207*, 143–154

Webster, L.A. & Kidnay, A.J. 2001: Vapor-liquid equilibria for the methane-propane-carbon dioxide systems at 230 K and 270 K. *Journal of Chemical & Engineering Data 46*, 759–764

Yokoyama, C., Wakana, S., Kaminishi, G. & Takahashi, S. 1988: Vapor-liquid equilibria in the methane-diethylene glycol-water system at 298.15 and 323.15 K. *Journal of Chemical and Engineering Data 33*, 274–276

Appendix: Nomenclature

$\tilde{a}^{res}$	dimensionless residual Helmholtz free energy
$B_{a\beta,i}$	bond fraction of type αβ in molecule of component i
c_i	constant for calculating , u k-1, or cross association parameters ε and κ
C_m	Molality
d	hydrated diameter
e	charge of an electron
$g^{SW}_{a\beta}$	square-well radial distribution function
g	gravitational acceleration constant
k	Boltzmann constant
$K_{a\beta}$	binary interaction parameter
K	absolute permeability
K_{rm}	relative permeability
m	segment number
m_i	segment number of component i
M_i	molecular weight (g cc^{-1}) number of component i
N_{Av}	Avogadro number,
n(i)	number of association sites of molecule i
P	pressure
P_c	capillary pressure
cij	charge of ion j
T	absolute temperature
T^*	dimensionless temperature (= kT u-1)
R	universal gas constant
r	distance between the segments
u	well depth of SW potential
u/k	segment energy
u_α	segment energy of segment α
$u_{\alpha\beta}$	well depth of SW potential for the α-β interaction
v^{oo}	segment volume
v_α	molar volume of segment α
X	dimensionless quantity (= κd)
xi	mole fraction of component i
x'_i	mole fraction of ion i on a solvent-free basis
x_α	segment fraction
$X^{A\alpha i}$	mole fraction of molecule of component i not bonded at side A of segment α

z_j	valence of the ion j
Z	compressibility factor
β	(kT)-1
ε	well depth of the association site-site potential
ε_w	dielectric constant of water
$\hat{\varphi}_i$	fugacity coefficient of component *i*
κ^{AB}	parameter related to the volume available for bonding between sites A and B
κ	Debye inverse screening length
λ	segment reduced range of the potential well
$\lambda_{\alpha\beta}$	reduced range of the potential well for the α-β interaction
ρ_m	molar density
ρ_n	number density
ρ^*	reduced density
σ_α	diameter of segment α
Γ	set of sites
τ	close-packed reduced density (= 21/2 π/6)
Δ_ρ	density difference
$\Delta^{A\alpha_i B_{\beta j}}$	association strength between site Aα at molecule of component i and site Bβ at molecule of component j